Highly localized positive contrast of small paramagnetic objects using 3D center-out RAdial Sampling with Off-resonance Reception (RASOR)

P. R. Seevinck[1], H. De Leeuw[1], C. Bos[2], and C. J. Bakker[1]

[1]Radiology, University Medical Center Utrecht, Utrecht, Netherlands, [2]Philips Healthcare, Best, Netherlands

INTRODUCTION- Accurate depiction and localization of small (super-) paramagnetic objects with MRI, such as paramagnetic markers, brachytherapy seeds and biopsy needles has been a challenge since the advent of MRI. Methods developed so far, including T_2^*-weighted imaging and positive contrast techniques like white marker, IRON and SGM, all suffer from the fact that the size and shape of the susceptibility artifact are generally not representative for the object. In this work we present a 3D imaging technique, applying RAdial Sampling with Off-resonance Reception (RASOR), to accurately depict and localize small paramagnetic objects with high positive contrast. The method will be demonstrated by 1D time domain simulations and experiments with a gel phantom containing three paramagnetic objects with very different geometry, viz, subvoxel stainless steel spheres, paramagnetic brachytherapy seeds and a puncture needle. The geometric accuracy of the RASOR method will be evaluated using computed tomography (CT) as the gold standard.

METHODS- The RASOR imaging technique is a fully frequency encoded 3D ultrashort TE (UTE) center-out acquisition method, which utilizes a large excitation bandwidth and off-resonance reception. Since local magnetic field distortions cause geometrical distortions parallel to the frequency encoding direction, radial signal pile-up may be expected when applying 3D center-out sampling in the presence of a small paramagnetic object. By manually introducing an offset, Δf_0, to the central reception frequency (f_0), the magnetic field disturbance causing the radial signal pile-up can be compensated for, resulting in a hyperintense signal at the exact location of the small paramagnetic object. Long T_2^* suppression can be accomplished by subtraction of a later echo.

Theory: A local magnetic field distortion $\Delta B(r)$, caused by a paramagnetic object, influences the local precession frequency according to: $\Delta f_{Larmor}(r)=\gamma/2\pi\,\Delta B(r)$. Manually changing the f_0 reception frequency may be regarded as imposing an offset to the magnetic field, yielding the following expression for the total field distortion: $\Delta B(r)_{total} = \Delta B(r)+\Delta f_0 2\pi/\gamma$. By introducing an offset Δf_0 of opposite sign, magnetic field distortions caused by paramagnetic perturbers can be balanced. This concept is demonstrated in the 1D imaging equation shown in Eq. [1], in which the first exponential term describes the combined influence of a local field distortion $\Delta B(r)$ and off-resonance reception on spatial encoding, the second exponential describes the influence of $\Delta B(r)$ on dephasing, G represents the imaging gradient and t'=t-TE,

$$s(t',G)=\int_0^\infty dr\;\rho(r)e^{-i\gamma G\,(r+(\Delta B(r)+\Delta f_0\cdot 2\pi/\gamma)/G)t'}e^{-i\gamma\,(\Delta B(r)+\Delta f_0\cdot 2\pi/\gamma)TE} \qquad [1]$$

Simulations: Radial center-out k-space sampling was simulated (Mathematica) on an axis perpendicular to B_0 according to Eq. [1] to generate the intensity profile of an object containing a spherical susceptibility inclusion with $\Delta\chi = 4000$ ppm and radius = 0.25 mm. A super-sampling factor of 10 was used to simulate intravoxel dephasing. Other parameters included FOV = 128; matrix = 128; TE/ΔTE=0.08/1.5 ms; B_0 = 3T. A read gradient of 24 mT/m was used.

In vitro experiments: 3D UTE MR experiments were conducted with and without off-resonance reception on a 3T system (Achieva, Philips Healthcare) using agarose gel (2%) phantoms doped with 12 mg/ml $MnCl_2$ ($R_2 \sim 30\ s^{-1}$), containing: a) stainless steel spheres (radius = 0.25 mm); b) paramagnetic brachytherapy seeds (4.5x0.8 mm); c) a puncture needle (Somatex®, diameter 18G~1.2 mm). The following imaging parameters were applied: FOV = 128 mm; matrix = 128^3 and TR/TE_1/TE_2 = 5.0/0.08/1.5 ms; read gradient = 24 mT/m (BW~1 kHz/pix); BW_{ex} ~ 40kHz; T_{Acq} = 2:43 min. Off-resonance values were optimized for each object by trial and error, resulting in -2 kHz for the stainless steel spheres and the puncture needle and -1 kHz for the brachytherapy seeds.

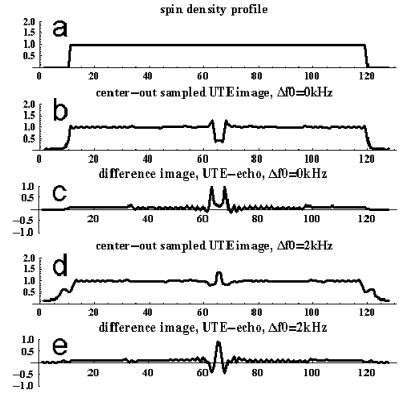

Fig.1. Simulations of center-out UTE and RASOR imaging

RESULTS-Simulations 1D simulations of a subvoxel paramagnetic sphere showed that center-out sampling causes hyperintensities to be generated on both sides of the signal void at the exact location of the disturber (Fig. 1b). Subtraction of an echo from the UTE image demonstrated signal pile up on both sides of the magnetized sphere, while suppressing the background signal (Fig. 1c). When applying an optimized f_0 offset a hyperintensity was created exactly at the location of magnetized sphere (Fig. 1d), while suppressing the background signal by subtraction of a later echo (Fig. 1e).

In vitro experiments: RASOR successfully generated highly localized hyperintensities for all paramagnetic perturbers. This is shown by transversal (a-e) and coronal (d, e, f) UTE (a, b) and RASOR (b, c, e, f) images of the stainless steel sphere in agarose in Fig. 2. Fig. 3 demonstrates MIP's of RASOR (a, c) and CT (b, d) images of the phantom with five stainless steel spheres. Very good agreement between UTE and CT was observed. After 3D rigid registration of the phantoms a mean error of 0.89 mm was found. RASOR successfully depicted brachytherapy seeds (Fig. 4a, b), irrespective of their orientation with respect to B_0. Good comparison with CT (Fig. 4b, d) was observed. Similar observations were done for a puncture needle in Fig. 5, showing good correspondence for both coronal and sagital RASOR (Fig 5a, b) and CT (c, d) images. A steel sphere was included as a reference as well.

DISCUSSION- The affectivity of the RASOR imaging method can be attributed to three factors. 1) The use of a hard, non-selective RF block pulse generates a large excitation bandwidth and excites the all spins in the volume of interest, also spins in the vicinity of (super-) paramagnetic objects which resonate at frequency offsets of several kHz; 2) Fully frequency encoded radial sampling of k-space, which causes a radial signal pile-up in the vicinity of a small magnetized object, the center of gravity of which coincides with the center of the magnetized object. In combination with off-resonance reception, applied to balance field distortions induced by the small magnetized object, this leads to a summation of the radial signal pile up exactly at the location of the small magnetized object, locally generating high positive contrast, possibly much higher than would be expected from the actual spin density. 3) The use of ultrashort echo times, which minimizes subvoxel dephasing in the vicinity of the magnetic perturbers, while geometrical distortions and signal pile-up are independent of the echo time and are in fact exploited in UTE RASOR imaging to generate high positive contrast. In conclusion, the presented RASOR imaging technique successfully exploits magnetic field distortions in the vicinity of small magnetized objects placed in a B_0 field, by generating high positive contrast exactly at the location of the magnetized object, while suppressing background signal.

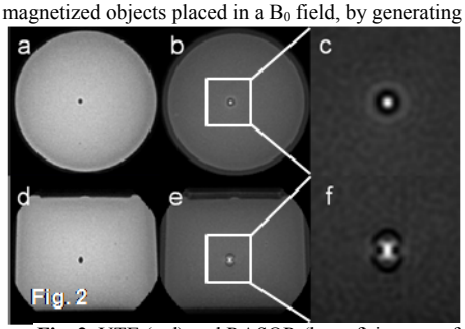

Fig. 2. UTE (a,d) and RASOR (b,c,e,f) images of the stainless steel sphere.

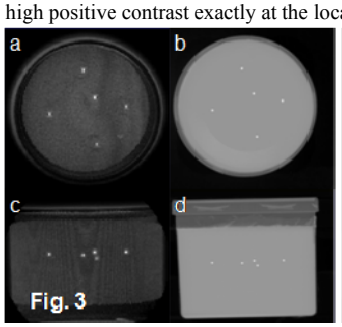

Fig. 3. RASOR (a, c) and CT (b, d) imagesof five stainless steel spheres.

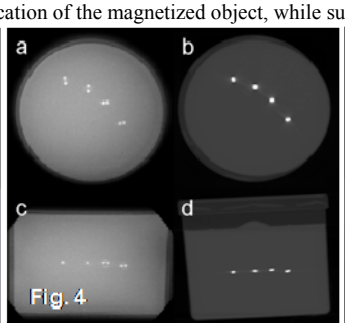

Fig. 4. RASOR (a, c) and CT (b, d) images of brachtherapy seeds.

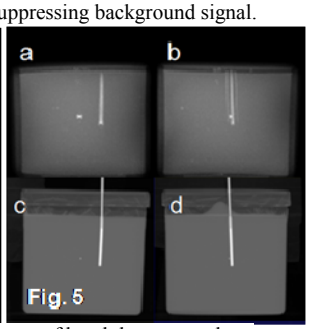

Fig. 5. RASOR (a, c) and CT (b, d) images of a puncture needle.